J Solid State Electrochem (2018) 22:537–546
https://doi.org/10.1007/s10008-017-3791-0

ORIGINAL PAPER

Lithium-sulphur batteries based on biological 3D structures

T. Kazda[1] · P. Čudek[1] · J. Vondrák[1] · M. Sedlaříková[1] · J. Tichý[1] · M. Slávik[2] · G. Fafilek[3] · O. Čech[1]

Received: 5 April 2016 / Revised: 26 September 2017 / Accepted: 30 September 2017 / Published online: 6 October 2017

Abstract Lithium-sulphur accumulators are, thanks to their high theoretical energy density and good availability of sulphur, one of the most promising concepts of the new generation of accumulators. In this paper, we present a 3D structured cathode formed on a natural basis. A sea sponge *Spongia officinalis* served as a template for the electrode structure. This 3D electrode provides enough space for sulphur. Thus, it allows high sulphur loading. This electrode structure also immobilizes polysulphides inside the cathode and improves stability during cycling. The resultant new cathode configuration allows reaching very high sulphur area loading of 4.9 mg/cm^2 which is almost four times more than in the case of a standard coated electrode. Despite the high sulphur loading, the electrode maintains high stability during cycling in comparison with a standard electrode and it also reaches much higher square capacity, exceeding 3.0 mAh/cm^2.

Keywords Lithium-ion battery · Lithium-sulphur battery · 3D cathode · Sulphur

✉ T. Kazda
kazda@feec.vutbr.cz

[1] Department of Electrical and Electronic Technology, Faculty of Electrical Engineering and Communication, Brno University of Technology, Technická 10, 616 00 Brno, Czech Republic

[2] Iontech Systems AG, Auerstrasse 19, 9435 Heerbrugg, Switzerland

[3] Institute of Chemical Technologies and Analytics, TU Vienna, Getreidemarkt 9/164ec, A-1060 Vienna, Austria

Introduction

Lithium-sulphur accumulators are one of the promising potential ways of commercial accumulators' development. These accumulators are very attractive, thanks to their high theoretical energy density, for use in electric vehicles and large stationary energy storage systems as well as in electric aircrafts [1]. Practical use of lithium-sulphur accumulators is very tempting because of the very high theoretical capacity of sulphur—1675 mAh/g which, in combination with the potential around 2.1 V against lithium, means that its gravimetric energy density reaches about 3000 Wh/kg [2, 3]. The theoretical capacity of sulphur is much higher than the capacity of presently available cathode materials as $LiMn_2O_4$ (148 mAh/g) [4], $LiFePO_4$ (170 mAh/g) [5] or $LiNi_{1/3}Mn_{1/3}Co_{1/3}O_2$ (280 mAh/g) [6, 7, 4]. Another advantage is good availability of sulphur, its low price and environmental friendliness [3]. However, there are several fundamental problems that must be solved before the commercial use of these batteries could begin. One of the biggest problems of this accumulator type is the fact that there is no intercalation process of lithium ions during cycling but conversion of materials occurs during cycling. The result of this conversion is a compound of sulphur and lithium—Li_2S (lithium sulphide). This conversion, from S_8 to Li_2S, proceeds in several steps. The first one is the formation of Li_2S_8, then there is the formation of Li_2S_6, Li_2S_4, Li_2S_2 and, finally, Li_2S. The resulting polysulphides, Li_2S_8 to Li_2S_4, are soluble in the electrolyte and they deposit on the anode surface of metal lithium during cycling which leads to a very steep drop of the capacity during cycling [8]. This process is known as the "shuttle effect" [9]. An additional disadvantage of the material is its low conductivity ($5 \cdot 10^{-30}$ S/cm) resulting from the fact that sulphur is an insulator [10, 11]. Another problem is volumetric expansion of the ma-

terial during cycling which leads to approximately 80% increase of volume. The consequence of that is the loss of contact between different parts of the electrode—sulphur and carbon [3, 6, 12–14]. Several teams of scientists around the world are trying to solve these problems using a wide variety of methods. One possibility is to encapsulate sulphur with carbon which prevents the release of polysulphides into the electrolyte and increases conductivity of the sulphur particles [15, 16]. Another option is encapsulation similar to the one from the previous example but with a polymer such as polyaniline, polythiophene or polypyrrole [17–19]. These polymers are conductive and prevent the dissolution of polysulphides into the electrolyte and these materials also have their own capacity [19]. Another possibility is the creation of a special 3D cathode structure into which sulphur is enclosed, thereby preventing the deposition of polysulphides at the anode side [20–22]. Other researchers solve this problem with polysulphides forming special active layers on the surface of the separator which works like a trap for polysulphides and prevents them from accessing the anode side [23].

Experimental

The *Spongia officinalis* sea sponge was used as a material for the preparation of a 3D structure which will serve as the basis for the electrode. The sponge was annealed at 800 °C for 30 min in nitrogen atmosphere. The aim was to preserve 3D structures during annealing and to convert the organic material of the sponge to a 3D structured carbon matrix. A thin slice was sliced off the annealed sea sponge and a circular electrode with the diameter of 12 mm was cut out of it. The thickness of the slice was ~ 300 μm. Conventional slurry for the preparation of sulphur electrode was mixed by a magnetic stirrer after annealing. The slurry consisted of the following: sulphur (Sigma-Aldrich, 99.5%), carbon Super P and polyvinylidene fluoride (PVDF) in the weight ratio of 60:30:10 dispersed in *N*-methyl-2-pyrrolidone (NMP). The slurry prepared this way was, after 24 h of stirring, impregnated into the 3D structured electrode using a syringe. This slurry was also deposited on Al foil by a coating bar in order to create classical electrodes for comparison. Both types of electrodes were dried in an oven at 60 °C for 24 h. Discs with the diameter of 12 mm were cut out from the prepared layer on Al foil and then pressed. They were, together with the 3D structured electrode, dried again in vacuum and then in an oven at 60 °C inside a glove box. Sulphur loading of the basic electrode was 1.4 mg/cm^2 and it was 4.9 mg/cm^2 in the case of the 3D structured electrode. The percentage of sulphur in the basic electrode including the Al collector was 18%. The percentage of sulphur in the case of the 3D structured electrode was 40% (including the carbon matrix). Both electrodes were then inserted into the electrochemical test cell ECC-STD (El-Cell©). The whole assembly was done in a glove box in argon atmosphere. Metal lithium was used as a counter electrode and 0.25 mol/l of lithium nitrate ($LiNO_3$, Sigma-Aldrich) + 0.7 mol/l of lithium bis(trifluoromethanesulfonyl)imide (LiTFSI, Sigma-Aldrich) solution in 1,2-dimethoxyethane (DME, Sigma-Aldrich) and 1,3-dioxolane (DOL, Sigma-Aldrich) was used as electrolyte where the ratio was DME:DOL 2:1 *v/v*. The electrolyte was impregnated into a glass fiber-based separator. Cyclic voltammetry (CV) and galvanostatic cycling were used for electrochemical characterization. Both methods were performed on the VMP3 potentiostat (Bio-Logic). CV was done in the

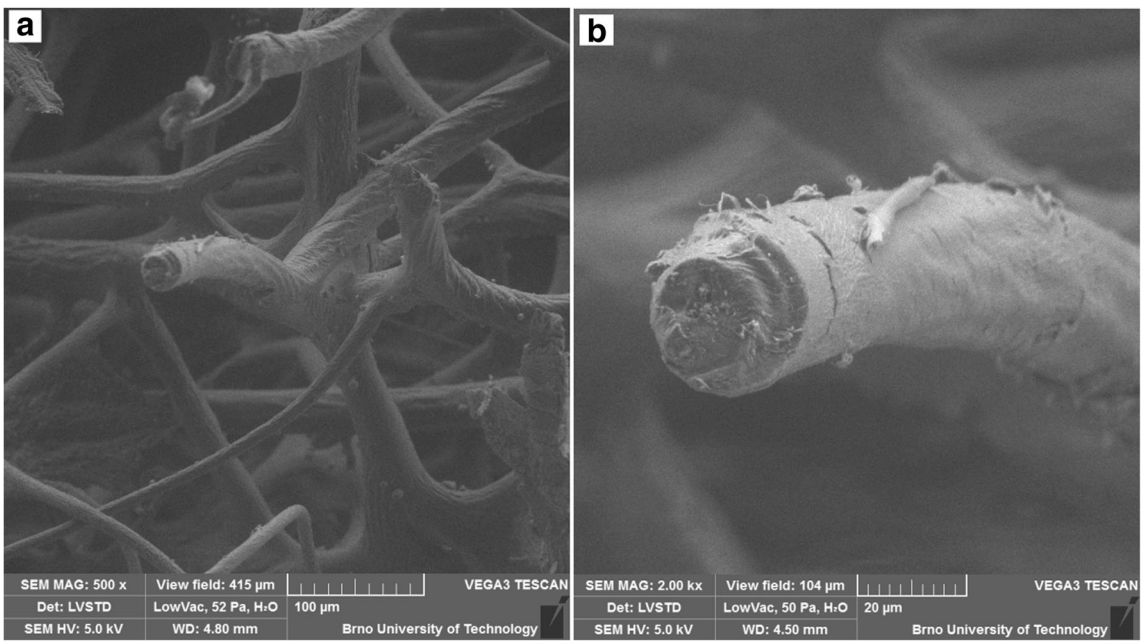

Fig. 1 SEM images of the *Spongia officinalis*. **a** Before annealing, used field of view: 415 μm. **b** Before annealing, used field of view: 104 μm

potential window from 1.8 to 3.0 V versus lithium and the scan rates were set to 1 and 0.1 mV/s. Galvanostatic cycling was carried out within a potential window from 1.8 to 2.8 V versus lithium. TESCAN VEGA3 XMU electron microscope (SEM) with Bruker EDAX analyzer was used for SEM and energy-dispersive X-ray spectroscopy (EDS) characterization. Kratos Ultra DLD spectrometer was used for X-ray photoelectron spectroscopy (XPS) analysis.

Results and discussion

We can see the structure of the *Spongia officinalis* sea sponge before annealing displayed by SEM in Fig. 1. Figure 1a shows SEM images of the sea sponge in 415 μm field of view. The figure clearly shows a complex sponge structure formed by a network of connected columns. Figure 1b shows one of these columns in detail. It is evident that the diameter of the column is about 30 μm. Images were taken in a high-pressure environment with evaporated water inside the microscope chamber due to the biological origin of the sample. The structure of the *Spongia officinalis* sea sponge after annealing can be seen in Fig. 2. It is evident that the complex structure of the sponge was preserved and the material of the sponge was changed to a conductive carbon structure which allows us to take pictures in vacuum (Fig. 2a). A closer look into the column reveals that the structure of the sponge was torn after annealing and the diameter of the column was reduced to approximately 15 μm (Fig. 2b). The surface of the column is shown in Fig. 2c. It is clearly visible that the surface is very wrinkled which indicates that there is a large number of small pores on the surface. We can see the detail of the surface in Fig. 2d. It shows that the pore size is in the range from tens to hundreds of nanometers. This extreme porosity should allow polysulphides to be captured in these pores and thus prevent capacity decrease of the electrode during cycling.

XPS was utilized in order to investigate the chemical composition of the *Spongia officinalis* after annealing (Fig. 3).

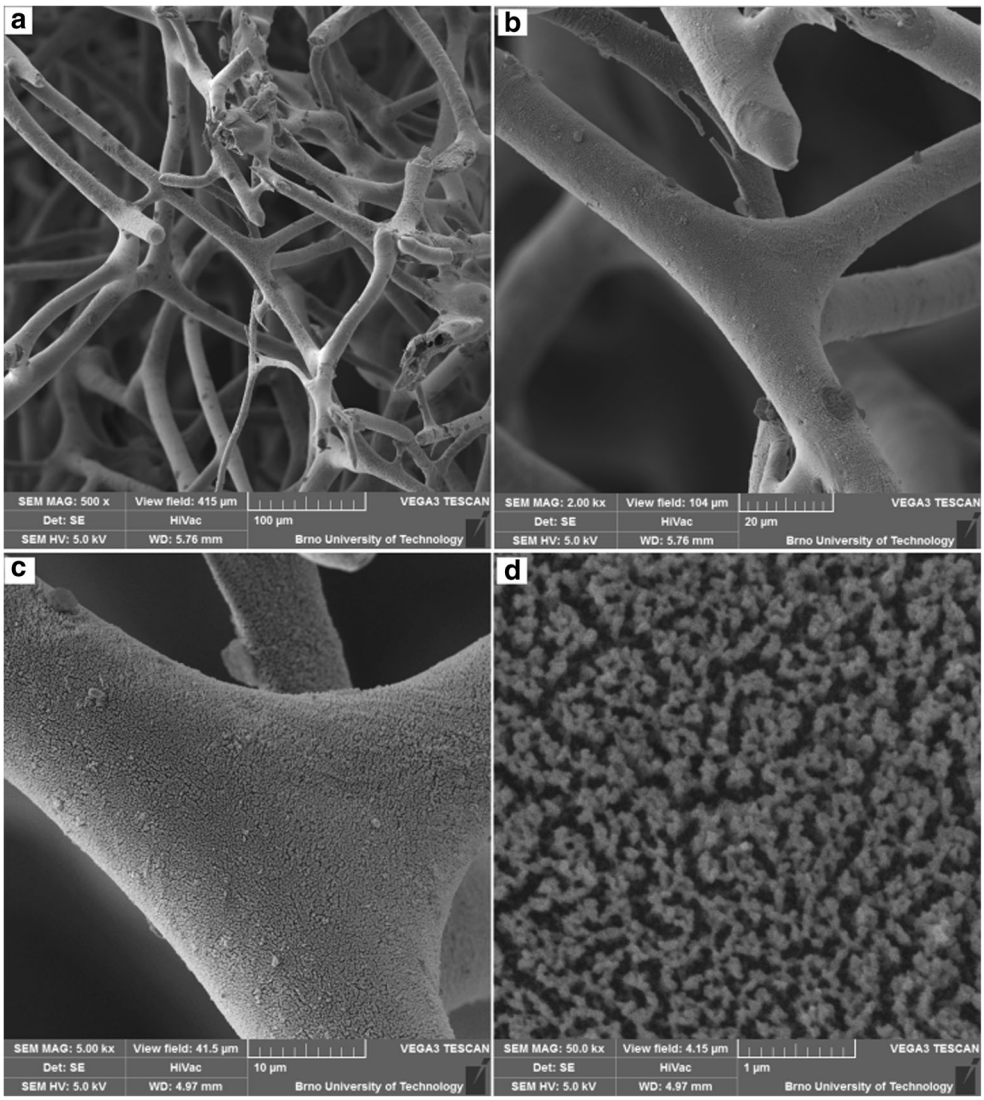

Fig. 2 SEM images of the *Spongia officinalis*. **a** After annealing, used field of view: 415 μm. **b** After annealing, used field of view: 104 μm. **c** After annealing, used field of view: 41.5 μm. **d** After annealing, used field of view: 4.15 μm

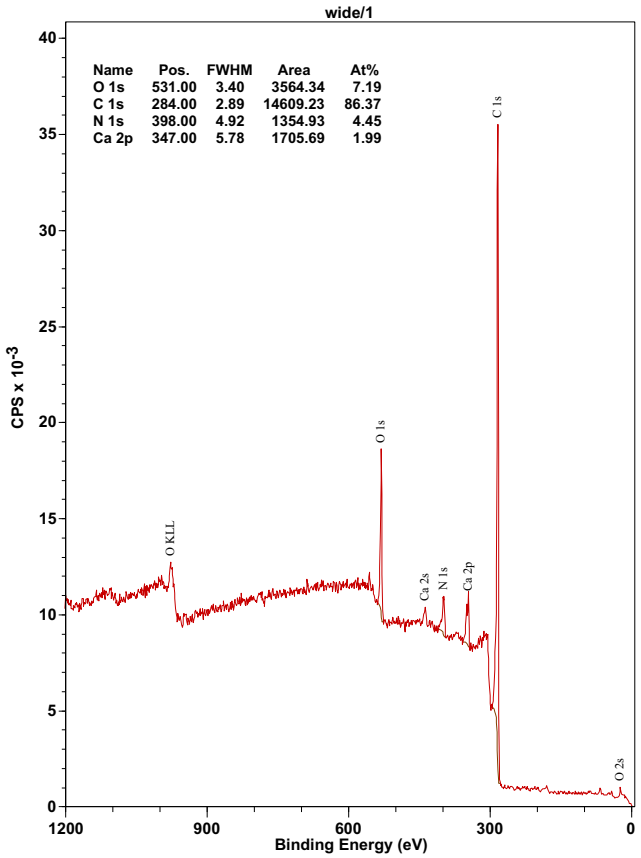

Fig. 3 XPS spectra of the *Spongia officinalis* after annealing

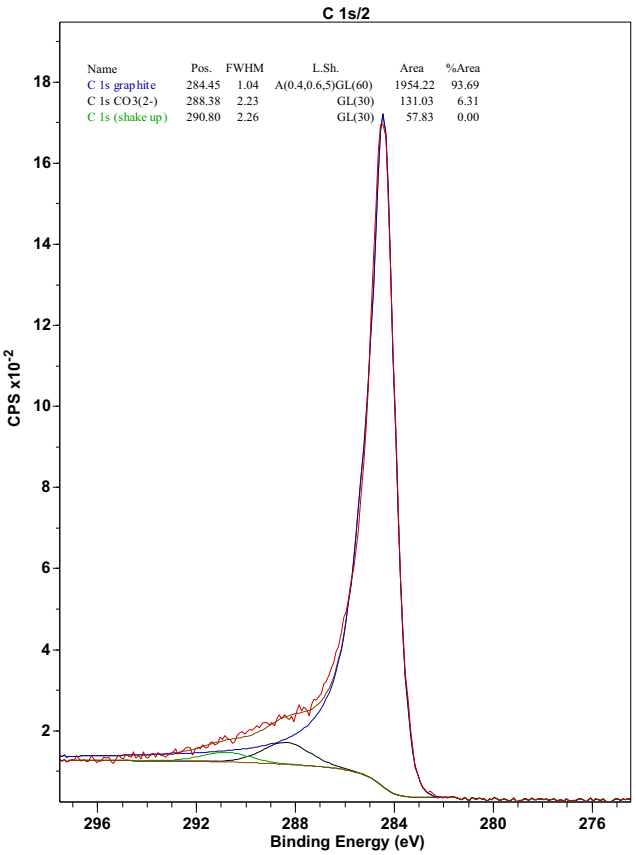

Fig. 4 XPS spectra of the carbon in the *Spongia officinalis* after annealing

XPS spectra revealed that the proportion of the carbon atoms was 86%. The rest of the *Spongia officinalis* after annealing was formed by oxygen, nitrogen and calcium. Obtained results confirmed the formation of C–N bonds during the annealing process. The advantage of nitrogen content is the fact that nitrogen is more electronegative than carbon which improves polysulphide adsorption [24, 25]. Nitrogen-doped carbon materials improve chemical absorption of sulphur and minimize sulphur loss during cycling [22, 26, 27]. The fitted carbon spectrum (Fig. 4) showed that the dominant component of this material is graphite, which is evident from the peak around 284 eV. Other peaks correspond to C=O and O–C=O bonds. Partial oxygen replacement and formation of the C–N bond occur due to the presence of nitrogen [22].

Figure 5 shows SEM images of the 3D structured electrode based on *Spongia officinalis* impregnated by the prepared slurry. The electrode slurry is retained on the surface of the individual columns and in the space between them (Fig. 5a). A slurry film on the surface of the columns is shown in Fig. 5b. When we look closely, we can see that the surface of the column is coated with the thin film of the slurry that is trapped in the pores on the surface of the columns (Fig. 5c, d). EDS analysis with surface mapping of the 3D structured electrode was performed together with the SEM analysis. The EDS mapping of the 3D structured electrode can be seen in Fig. 6. Figure 6a displays the analysed area of the 3D structured electrode. Figure 6b shows the distribution of carbon and sulphur in the 3D structured electrode. It is evident that the structure of the sponge after annealing is formed by carbon which is at some locations covered with sulphur contained in the slurry and also that sulphur is closed in the space between columns like in a cage.

Figure 7a presents the comparison of CV curves for the S + Super P + PVDF electrode and the 3D structured electrode at the scan rate of 1 mV/s. The current axis is related to 1 g of sulphur. CV shows that the size of current peaks is almost the same which means that sulphur utilization in both electrodes is the same despite the high sulphur loading in the 3D structured electrode (4.9 mg/cm^2) compared to 1.4 mg/cm^2 in the standard S + Super P + PVDF electrode. However, the kinetic of the reaction at this scan rate of the 3D structured electrode is slower than the kinetic of the S + Super P + PVDF electrode. We can clearly see that the anodic peak of the 3D structured electrode is shifted to higher potential than the anodic peak of S + Super P + PVDF electrode. Similarly, in the case of cathodic peaks of the S + Super P + PVDF electrode, two cathodic peaks can be clearly seen and in the case of the 3D structured electrode, we can see just the first peak and the

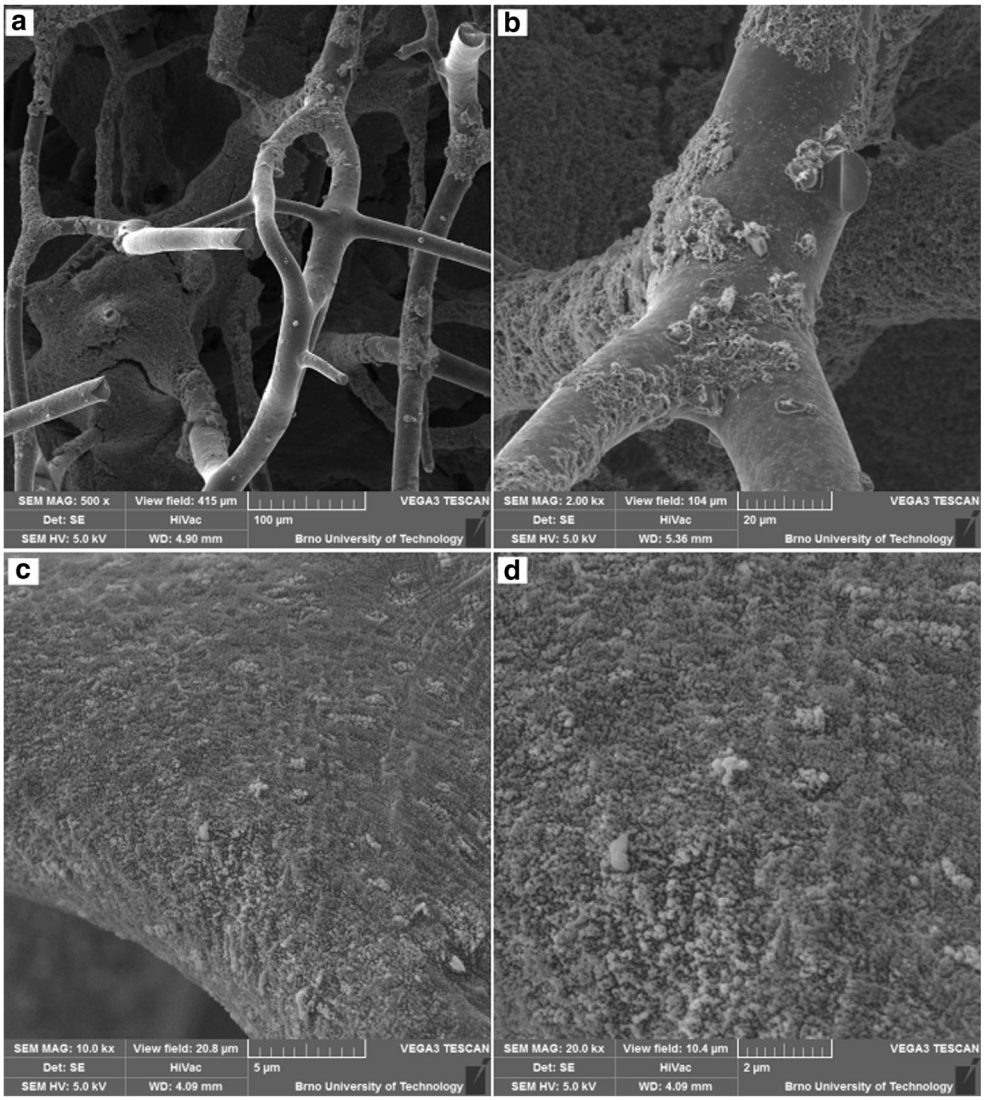

Fig. 5 SEM images of the 3D structured electrode based on *Spongia officinalis* impregnated by slurry. **a** 3D structured electrode, used field of view: 415 µm. **b** After annealing, used field of view: 104 µm. **c** After annealing, used field of view: 41.5 µm. **d** Before annealing, used field of view: 4.15 µm

beginning of the second peak. Figure 7b presents the comparison of one CV curve for the S + Super P + PVDF electrode and the 3D structured electrode at the slow scan rate of 0.1 mV/s. The current axis is related to square centimetre of electrode. We can see oxidation and reduction peaks for both electrodes. We can also see two cathodic peaks at 2.4 and 2.0 V, which are related to the reduction of elemental sulphur to higher-order lithium polysulphides and then their reduction to lower-order lithium polysulphides in both electrodes [28, 29]. Positions of the anodic and cathodic peaks

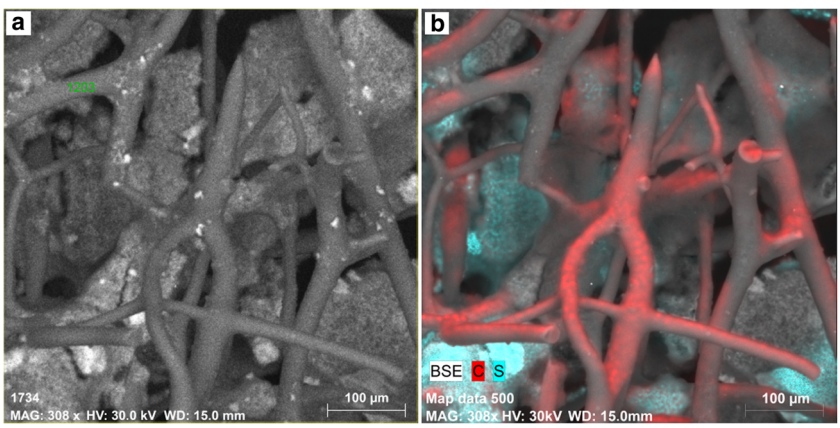

Fig. 6 EDS mapping of the 3D structural electrode based on *Spongia officinalis* impregnated by slurry. **a** SEM image of 3D structured electrode. **b** Distribution of carbon and sulphur

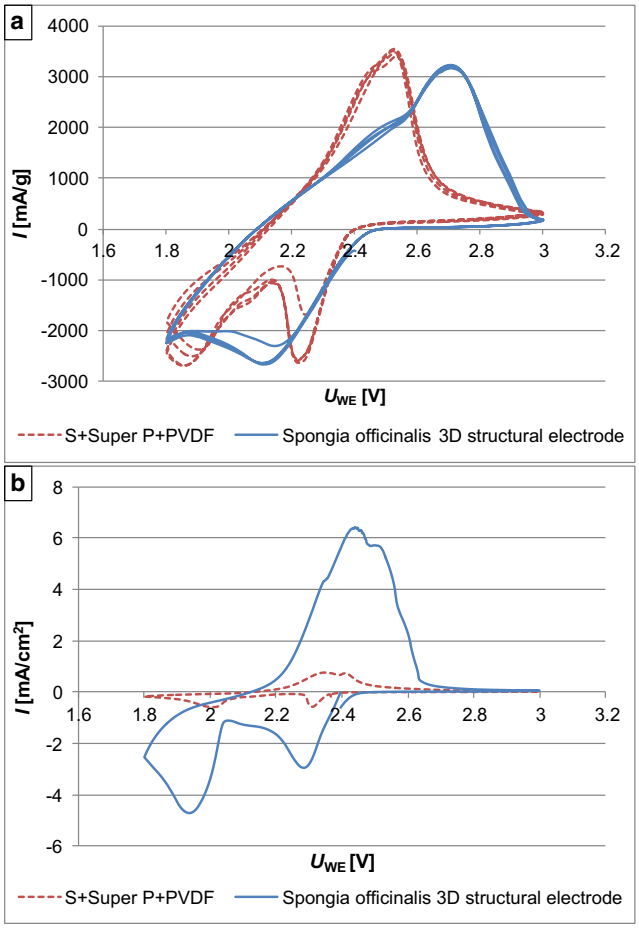

Fig. 7 CV of **a** *Spongia officinalis* 3D structured electrode and S + Super P + PVDF electrode, scan rate 1 mV/s with current axis per gram, and **b** *Spongia officinalis* 3D structured electrode and S + Super P + PVDF electrode, scan rate 0.1 mV/s with current axis per square centimetre

for S + Super P + PVDF and 3D structured electrode are almost the same which means that the slower kinetics of the 3D structured electrode does not apply at this scan rate. However, the current per square centimetre of the electrode reached significantly higher values in the case of 3D structured electrode than the current for the standard electrode. This is caused by the higher sulphur loading and its utilization comparable with the standard electrode.

The next performed investigation was galvanostatic cycling and cycling at various C-rates. Capacity retention and efficiency during galvanostatic cycling for the S + Super P + PVDF electrode and the 3D structured electrode are displayed in Fig. 8a. The 3D structured electrode showed a high drop of capacity during the first three cycles of cycling at 0.2 C. However, the decrease of capacity subsequently stopped. The cells with the S + Super P + PVDF and 3D structured electrode delivered initial discharge-specific capacities of 782 and 637 mAh/g at 0.2 C. The specific capacity of the 3D structured electrode was smaller than the capacity of the S + Super P + PVDF electrode. However, the capacity drop between cycle numbers 10 and 20 was 4% for the S + Super P + PVDF electrode and it was 1.4% for the 3D structured electrode. During the first 20 cycles, the 3D structured electrode reached coulombic efficiency more than 97% and the S + Super P + PVDF electrode showed efficiency around 94%. Rate performance was measured after the first 20 cycles by cycling at various C-rates up to 2 C. The increase of the C-rate was followed by its reduction to the original value 0.2 C (the same step size). The discharge capacity of the S + Super P + PVDF electrode decreased to 574 and 429 mAh/g at 0.5 and 1 C which is a decrease of 26.7 and 45.2%, respectively, in comparison with the capacity of the first cycle. In the case of the 3D structured electrode, the decrease was much smaller: 13.3 and 23.2% at 0.5 and 1 C, respectively. This corresponds to the capacity of 553 and 490 mAh/g. A significant decrease of discharge capacity for both the electrodes was observed at the higher C-rate—2 C. The S + Super P + PVDF electrode delivered 280 mAh/g and the 3D structured electrode delivered 155 mAh/g which corresponds to 64 and 75% capacity loss. At this C-rate, a worse kinetic of the 3D structured electrode can be seen, which corresponds to the data obtained by cyclic voltammetry. The results show that the 3D structured electrode is more stable than the conventional electrode but within a certain limit which is the current 2 C. However, the 3D structured electrode had a tendency to adapt to this load change as the capacity increased over five cycles, probably due to the gradual improvement of the contact between sulphur and electrolyte at this high C-rate [30]. Similar results were obtained by Yan [31]—he reported high discharge capacity difference between cycling at 1 and 2.5 C with multilayered cathode with sulphur loading 1.85 mg/cm^2. At the beginning of cycling, the capacity was approx. 650 mAh/g at 1 C and 150 mAh/g at 2.5 C. However, the capacity at 2.5 C was also growing during cycling.

Nevertheless, the 3D structured electrode provided better stability during the subsequent reduction of the C-rate at 1, 0.5 and 0.2 C because the obtained capacity was similar to the capacity from the previous cycling, unlike the S + Super P + PVDF electrode where a decrease of capacity was observed. Capacity of the 3D structured electrode after 50 cycles was 562 mAh/g, corresponding to 88% capacity retention. Capacity of the S + Super P + PVDF electrode was 667 mAh/g, corresponding to 85% capacity retention. The 3D structured electrode exhibited very stable capacity during cycling. The capacity decreased by approximately 15.8% after 80 cycles and the capacity of 537 mAh/g was reached in the last cycle. In the case of the S + Super P + PVDF electrode, capacity in the last cycle was 581 mAh/g and capacity decreased by 25.6%. Similar capacity decrease of a standard sulphur electrode was reported by Yao et al. [23] or Zhang et al. [32]. Coulombic efficiency

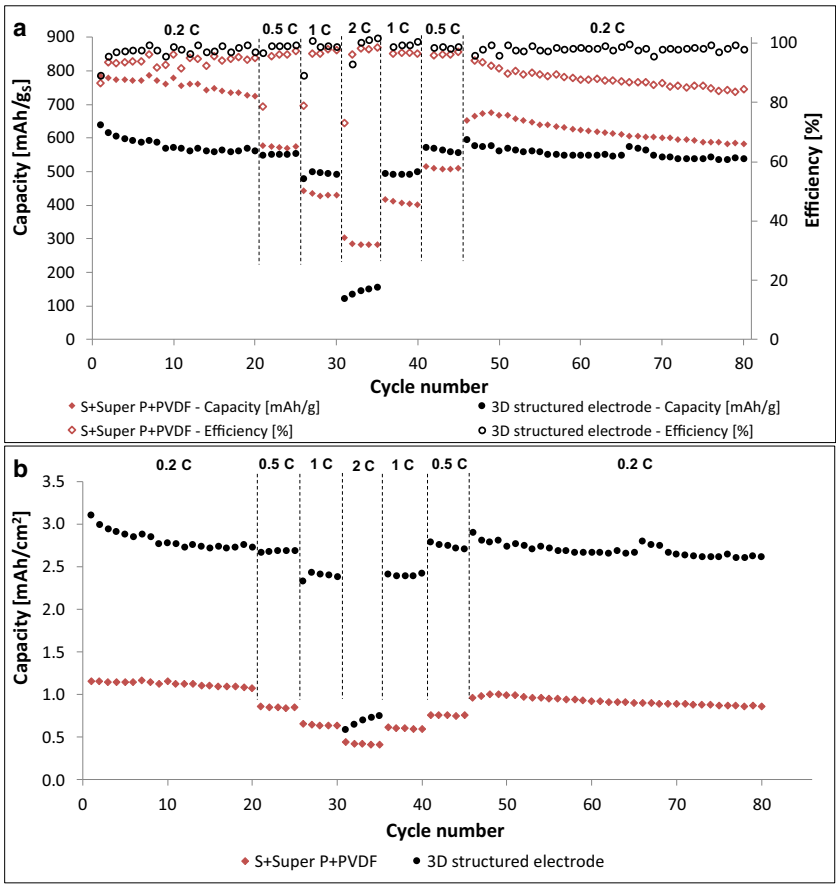

Fig. 8 Comparison of capacity changes during cycling of *Spongia officinalis* 3D structured electrode and S + Super P + PVDF electrode. **a** Capacity per gram. **b** Capacity per square centimetre

of the 3D structured electrode was, during the whole cycling, between 97 and 98%. This stable and high coulombic efficiency may be associated with the contents of 3D carbon sponge structure and nitrogen, which can conduct and trap polysulphides. Coulombic efficiency of the S + Super P + PVDF electrode was around 94% at the beginning of cycling and it dropped during the cycling down to 84%. Capacities achieved during cycling and at the end of cycling for every current load for the S + Super P + PVDF electrode and the 3D structured electrode are listed in Table 1. When we compare the results of the 3D structured electrode with the results of Ahn et al. [33], it is obvious that the 3D structured electrode achieved higher stability. Ahn reported capacity retention 71% after 100 cycles at 0.1 C with sulphur nanogranular film-coated three-dimensional graphene sponge composite (3D-GS) with sulphur mass loading of just 0.72–0.74 mg/cm^2. Walle et al. [34] reported, in their article about 3D sulphur/graphene/multiwalled carbon nanotube, cathode capacity loss 40% after 26 cycles at 0.2 C and 23.6% after 100 cycles at 0.8 C. Again, it is obvious that the 3D structured electrode based on *Spongia officinalis* is more stable.

Table 1 Capacities and capacity decrease during cycling of the 3D structured electrode and S + Super P + PVDF electrode

S + Super P + PVDF electrode									
C-rates	0.2 C		0.5 C	1 C	2 C	1 C	0.5 C	0.2 C	0.2 C
Cycle number	1	20	25	30	35	40	45	50	80
Capacity [mAh/g_s]	781.8	723.9	577.4	428.5	280.1	399.1	509.2	667.1	581.7
Capacity decrease versus 1st cycle (%)		− 7.4	− 26.7	− 45.2	− 64.2	− 49.0	− 34.9	− 14.7	− 25.6
3D structured electrode									
C-rates	0.2 C		0.5 C	1 C	2 C	1 C	0.5 C	0.2 C	0.2 C
Cycle number	1	20	25	30	35	40	45	50	80
Capacity [mAh/g_s]	637.4	560.7	552.6	489.7	155.1	497.4	556.0	561.8	536.9
Capacity decrease versus 1st cycle (%)		− 12.0	− 13.3	− 23.2	− 75.7	− 22.0	− 12.8	− 11.9	− 15.8

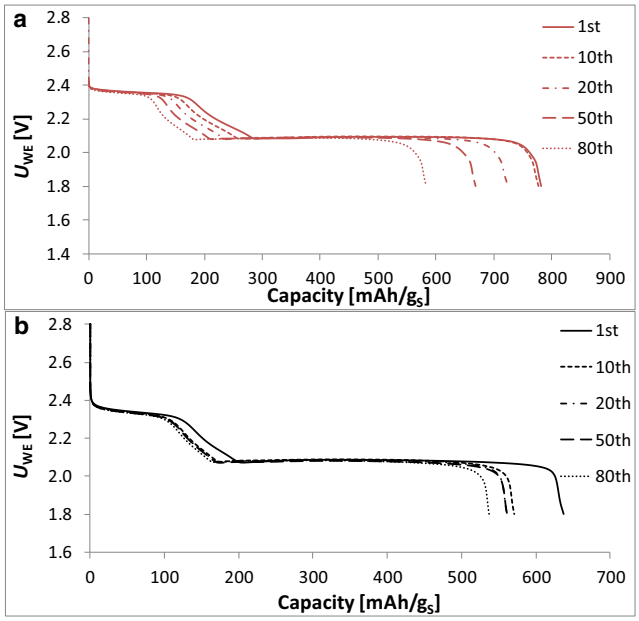

Fig. 9 Comparison of discharge curves of **a** S + Super P + PVDF electrode and **b** *Spongia officinalis* 3D structured electrode during cycling

Figure 8b shows the same cycling but with capacity calculated per square centimetre of electrode. The 3D structured electrode reached, thanks to the high loading of sulphur, much higher capacity per square centimetre than the S + Super P + PVDF electrode. The capacity of the 3D structured electrode at the beginning of cycling was 3.10 mAh/cm^2 and at it was 2.61 mAh/cm^2 at the end of cycling. The S + Super P + PVDF electrode reached the capacity of 1.16 mAh/cm^2 at the beginning of cycling and 0.86 mAh/cm^2 at the end of cycling. Similar results were achieved in an article from He et al. [21], where they used three-dimensional graphene-sulphur (3DGS) electrode and they achieved capacity around 700 mAh/g at 0.2 C and around 600 mAh/g at 0.5 C but the sulphur loading was only 1.0 mg/cm^2. Mi et al. [26] reported, in their article about N-doped 3D carbon foam/sulphur cathode, capacity retention 87% after 95 cycles at 0.2 C and capacity 632 mAh/g on the beginning of the cycling with coulombic efficiency 97%. These results are comparable with the results presented in this paper but sulphur loading including carbon foam was 36% and in this paper it is 40%. Nazar et al. [35] reported capacity up to 3 mAh/cm^2 at 0.2 C with sulphur loading of 5 mg/cm^2 with nanoporous graphitic carbon nitride g-C_3N_4. The data reported by Nazar are similar to the data in this article.

Figure 9a, b shows discharge curves for the S + Super P + PVDF and 3D structured electrodes during the whole cycling at 0.2 C. The results show that the 3D structured electrode maintains its stability as well as a stable plateau at 2.4 V. This plateau noticeably decreases in the case of the S + Super P + PVDF electrode. This plateau is connected to the reduction of elemental sulphur to higher-order lithium polysulphides Li_2S_8 and Li_2S_6 which are soluble in the electrolyte. This decrease does not occur in the case of the 3D structured electrode, possibly because the polysulphides are captured in the nitrogen-doped porous structure of the electrode surface. A similar phenomenon was presented by Babu [20] in his article about how they catch polysulphides inside a high-porous 3D nickel current collector. Babu reported somewhat higher capacity in his article (around 600 mAh/g_s at 0.2 C and around 500 mAh/g_s at 0.5 C) but the sulphur loading was 1.5 mg/cm^2 while it was 4.9 mg/cm^2 in our article. It follows that the capacity achieved per square centimetre of electrode during our experiments is more than three times higher. Liang et al. [36] reported capacity 910 mAh/g_s at the beginning of the cycling at 0.2 C and capacity around 500 mAh/g_s after 50 cycles with sulphur loading 5.5 mg/cm^2 which is similar loading like in this article but the capacity retention is much lower than the capacity retention presented in the current article.

Figure 10 shows SEM and EDS images of the 3D structured electrode based on *Spongia officinalis* impregnated by the prepared slurry after cycling. As we can see, sulphur is still kept inside the 3D structured electrode and on the surface of the pillars.

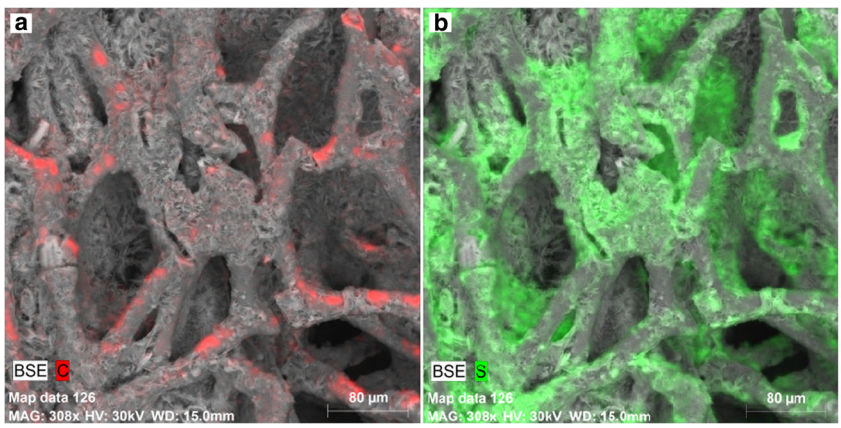

Fig. 10 EDS mapping of the 3D structural electrode based on *Spongia officinalis* impregnated by slurry after cycling. **a** SEM image of 3D structured electrode and distribution of carbon. **b** SEM image of 3D structured electrode distribution sulphur

Conclusions

It was clearly demonstrated that a readily available, low-cost and environmentally friendly material of the sea sponge *Spongia officinalis* can be used as a conductive matrix for electrodes of lithium-sulphur accumulators. The biological material of the sea sponge was, using a very simple method, converted to a conductive carbon network with high concentration of nanopores on the surface. Although the most basic possible electrode slurry consisting of the basic binder PVDF and the Super P carbon was used, we achieved extremely high loading of sulphur—almost 5 mg/cm^2 in the 3D structured electrode based on the sea sponge. It also achieved good stability during cycling and very high capacity per square centimetre up to 3.1 mAh/cm^2. It is clear from the discharge characteristics that the 3D structured electrode prevents the release of the polysulphides into the electrolyte. This is probably due to the presence of nitrogen inside the 3D carbon matrix which improves the polysulphide retention inside the electrode. This material could therefore eliminate the problems of stability and capacity loss at higher area sulphur loadings connected to lithium-sulphur accumulators. For its practical use, it would be necessary to modify the sponge growth system since it is barely uniform in its entire volume and so the volume from which can be formed electrodes with the greatest possible uniformity is very limited.

Acknowledgements This research has been carried out in the Centre for Research and Utilization of Renewable Energy (CVVOZE).

Funding information The authors gratefully acknowledge the financial support from the Ministry of Education, Youth and Sports of the Czech Republic under NPU I programme (project no. LO1210).

References

1. Manthiram A, Fu Y, Chung S, Zu C, Su Y (2014) Rechargeable lithium–sulfur batteries. Chem Rev 114:11751–11787
2. J. Kim, D. Lee, H. Jung, Y. Sun, J. Hassoun, B. Scrosati, An advanced lithium-sulfur battery, Adv Funct Materials. vol. 23 (2013) 1076–1080.
3. Yoo H, Markevich E, Salitra G, Sharon D, Aurbach D (2014) On the challenge of developing advanced technologies for electrochemical energy storage and conversion. Mater Today 17:110–121
4. Brodd R (2013) Batteries for sustainability: selected entries from the Encyclopedia of Sustainability Science and Technology. Springer-Verlag New York, New York
5. Fedorková A, Nacher-Alejos A, Gómez-Romero P, Oriňáková R, Kaniansky D (2010) Structural and electrochemical studies of PPy/PEG-LiFePO4 cathode material for Li-ion batteries. Electrochim Acta 55:943–947
6. Nitta N, Wu F, Lee J, Yushin G (2015) Li-ion battery materials: present and future. Mater Today 18:252–264
7. Fedorková A, Oriňáková R, Čech O, Sedlaříková M (2013) New composite cathode materials for Li/S batteries: a review. Int J Electrochem Sci 8
8. Assary R, Curtiss L, Moore J (2014) Toward a molecular understanding of energetics in Li–S batteries using nonaqueous electrolytes: a high-level quantum chemical study. J Phys Chem 118: 11545–11558
9. Y. Yin, S. Xin, Y. Guo, L. Wan, Lithium-sulfur batteries: electrochemistry, materials, and prospects, Angewandte Chemie. 50 (203) 13186–13200
10. Choi Y, Kim K, Ahn H, Ahn J (2008) Improvement of cycle property of sulfur electrode for lithium/sulfur battery. J Alloys Compd 449:313–316
11. Cao Z, Ma C, Jia Y, Sun Z, Yue H, Yin Y, Yang S (2015) Activated clay of nest structure encapsulated sulfur cathodes for lithium–sulfur batteries. RSC Adv 36:28349–28353
12. Manthiram A, Fu Y, Su Y (2013) Challenges and prospects of lithium–sulfur batteries. Accounts Chem Res 46:1125–1134
13. Evers S, Nazar L (2013) New approaches for high energy density lithium–sulfur battery cathodes. Accounts Chem Res 46:1135–1143
14. Yamin H, Peled E (1983) Electrochemistry of a nonaqueous lithium/sulfur cell. J Power Sources 9:281–287
15. Zhao X, Tu J, Lu Y, Cai J, Zhang Y, Wang X, Gu C (2013) Graphene-coated mesoporous carbon/sulfur cathode with enhanced cycling stability. Electrochim Acta 113:256–262
16. Wang X, Zhang Z, Yan X, Qu Y, Lai Y, Li J (2015) Interface polymerization synthesis of conductive polymer/graphite oxide@sulfur composites for high-rate lithium-sulfur batteries. Electrochim Acta 155:54–60
17. Xiao L, Cao Y, Xiao J, Schwenzer B, Engelhard M, Saraf L, Nie Z, Exarhos G, Liu J (2012) A soft approach to encapsulate sulfur: polyaniline nanotubes for lithium-sulfur batteries with long cycle life. Adv Mater 24:1176–1181
18. Wu F, Chen J, Chen R, Wu S, Li L, Chen S, Zhao T (2011) Sulfur/polythiophene with a core/shell structure: synthesis and electrochemical properties of the cathode for rechargeable lithium batteries. J Phys Chem C 115:6057–6063
19. Cheng H, Wang S (2014) Recent progress in polymer/sulphur composites as cathodes for rechargeable lithium–sulphur batteries. J Mater Chem A 2:13783
20. Babu G, Ababtain K, Ng K, Arava L (2015) Electrocatalysis of lithium polysulfides: current collectors as electrodes in Li/S battery configuration. Scientific Reports 5:8763
21. He J, Chen Y, Li P, Fu F, Wang Z, Zhang W (2015) Three-dimensional CNT/graphene–sulfur hybrid sponges with high sulfur loading as superior-capacity cathodes for lithium–sulfur batteries. J Mater Chem A 3:18605–18610
22. Zhou G, Paek E, Hwang G, Manthiram A (2015) Long-life Li/polysulphide batteries with high sulphur loading enabled by lightweight three-dimensional nitrogen/sulphur-codoped graphene sponge. Nat Commun 6:7760–7771
23. Yao H, Yan K, Li W, Zheng G, Kong D, Seh Z, Narasimhan V, Liang Z, Cui Y (2014) Improved lithium–sulfur batteries with a conductive coating on the separator to prevent the accumulation of inactive S-related species at the cathode–separator interface. Energy Environ Sci 7:3381–3390
24. Li Y, Fan J, Zheng M, Dong Q (2016, 2016) A novel synergistic composite with multi-functional effects for high-performance Li–S batteries. Energy Environ Sci:1998–2004
25. Chen J, Yuan R, Feng J, Zhang Q, Huang J, Fu G, Zheng M, Ren B, Dong Q (2015, 2015) Conductive Lewis base matrix to recover the missing link of Li2S8 during the sulfur redox cycle in Li–S battery. Chem Mater:2048–2055
26. Mi L, Xiao W, Cui S, Hou H, Chen W (2016, 2016) An N-doped three dimensional flexible carbon/sulfur cathode for lithium sulfur battery design. Dalton Trans:3305–3309
27. See K, Jun Y, Gerbec J, Sprafke J, Wudl F, Stucky G, Seshadri R (2014) Sulfur-functionalized mesoporous carbons as sulfur

hosts in Li–S batteries: increasing the affinity of polysulfide intermediates to enhance performance. Appl Mater Interfaces 6:10908–10916
28. Rao M, Li W, Cairns E (2012) Porous carbon-sulfur composite cathode for lithium/sulfur cells. Electrochem Commun 17:1–5
29. Guo J, Xu Y, Wang C (2011) Sulfur-impregnated disordered carbon nanotubes cathode for lithium–sulfur batteries. Nano Lett 11:4288–4294
30. Ryu H, Guo Z, Ahn H, Cho G, Liu H (2009) Investigation of discharge reaction mechanism of lithium|liquid electrolyte|sulfur battery. J Power Sources 189:1179–1183
31. Yan J, Liu X, Yao M, Wang X, Wafle T, Li B (2015) Long-life, high-efficiency lithium–sulfur battery from a nanoassembled cathode. Chem Mater 27:5080–5087
32. Zhang Z, Zhang Z, Wang X, Li J, Lai Y (2014) Enhanced electrochemical performance of sulfur cathode by incorporation of a thin conductive adhesion layer between the current collector and the active material layer. J Appl Electrochem 44:607–611
33. Ahn W, Seo M, Jun Y, Lee D, Hassan F, Wang X, Yu A, Chen Z (2016) Sulfur nanogranular film-coated three-dimensional graphene sponge-based high power lithium sulfur battery. ACS Appl Mater Interfaces 8:1984–1991
34. Walle M, Zhang Z, You X, Zhang M, Chabu J, Li Y, Liu Y (2016) Soft approach hydrothermal synthesis of a 3D sulfur/graphene/multiwalled carbon nanotube cathode for lithium–sulfur batteries. RSC Adv 6:78994–78998
35. Pang Q, Nazar L (2016) Long-life and high-areal-capacity Li–S batteries enabled by a light-weight polar host with intrinsic polysulfide adsorption. ACS Nano 10:4111–4118
36. Liang X, Rangom Y, Kwok C, Pang Q, Nazar L (2017) Interwoven MXene nanosheet/carbon-nanotube composites as Li-S cathode hosts. Adv Mater 29:1603040